CORA Cork Open Research Archive
Cartlann Taighde Oscailte Chorcaí

Title	Mechanism that dictates pore width and <111>a pore propagation in InP
Author(s)	Lynch, Robert P.; Quill, Nathan; O'Dwyer, Colm; Nakahara, Shohei; Buckley, D. Noel
Publication date	2012-03-15
Original citation	Lynch, R. P., Quill, N., O'Dwyer, C., Nakahara, S. and Buckley, D. N. (2012) 'Mechanism that dictates pore width and <111>a pore propagation in InP'. ECS Transactions, 50(6), pp. 319-334. http://ecst.ecsdl.org/content/50/6/319.abstract
Type of publication	Article (peer-reviewed)
Link to publisher's version	http://ecst.ecsdl.org/content/50/6 http://dx.doi.org/10.1149/05006.0319ecst Access to the full text of the published version may require a subscription.
Rights	© The Electrochemical Society
Item downloaded from	http://hdl.handle.net/10468/2828

UCC
University College Cork, Ireland
Coláiste na hOllscoile Corcaigh

Mechanism that Dictates Pore Width and <111>A Pore Propagation in InP

Robert P. Lynch, Nathan Quill, Colm O'Dwyer,[a] Shohei Nakahara and D. Noel Buckley

Materials and Surface Science Institute, and Department of Physics and Energy,
University of Limerick, Limerick, Ireland
[a] Present address: *Department of Chemistry, University College Cork, Cork, Ireland and Micro & Nanoelectronics Centre, Tyndall National Institute, Lee Maltings, Cork, Ireland*

We report a mechanism for pore growth and propagation based on a three-step charge transfer model. The study is supported by electron microscopy analysis of highly doped n-InP samples anodised in aqueous KOH. The model and experimental data are used to explain propagation of pores of characteristic diameter preferentially along the <111>A directions. We also show evidence for deviation of pore growth from the <111>A directions and explain why such deviations should occur. The model is self-consistent and predicts how carrier concentration affects the internal dimensions of the porous structures.

Introduction

Porosity in electrochemically etched semiconductors has been extensively investigated in the case of silicon (1) and to a lesser extent in the case of III-V compounds such as GaAs (2,3) and InP (4,5). Anion type and concentration can play a significant role in affecting the pore growth and morphology (6,7). The depth of porous layers and their preferential crystallographic growth directions have been shown to be affected by electrolyte type (8,9) and concentration (10), temperature (11), substrate type (12), orientation (13) and doping density (14).

We have previously investigated (15-19) the early stages of anodic formation of porous InP in aqueous KOH electrolytes and reported transmission electron microscopy (TEM) and scanning electron microscopy (SEM) evidence that clearly shows individual nanoporous domains. These nanoporous domains form from the propagation of pores along the <111>A directions. These pores originate from pits in the surface, branch to form porous domains beneath a thin (~40 nm) dense near-surface layer and eventually these domains merge to create a continuous porous layer (19). The nanoporous domains have triangular $(01\bar{1})$ cross-sections, 'dove-tail' (011) cross-sections and rectangular profiles when (100) planes are viewed in parallel to the electrode surface. However at higher potentials pore propagation can be forced to grow perpendicular to the electrode surface and at even higher potentials planar etching can occur (17). Indeed, not only variation of potential but also variation of electrolyte concentration can result in a gradual change in the etching mechanism from pore formation to planar etching as the KOH concentration is decreased to below 2 mol dm^{-3} (10,11,18).

This paper describes an investigation by SEM and TEM of pore propagation in n-InP anodized in KOH and presents a model – based on a three-step charge transfer mechanism – that describes why preferential propagation along <111>A crystallographic directions and branching of pores occur. The model also accounts for the initial $[\bar{1}00]$ growth of pits, variation of the pore diameter with carrier concentration and deviation of pore propagation from the <111>A directions.

Experimental

The working electrode consisted of polished (100)-oriented monocrystalline sulfur-doped n-type InP. An ohmic contact was made to the back of the InP sample and isolated electrically from the electrolyte by means of a suitable varnish. The electrode area was typically 0.2 cm^2. InP wafers with carrier concentrations from 3.4-6.7 $\times 10^{18}$ cm^{-3} and etch pit densities < 5000 cm^{-2} were used. Anodization was carried out in aqueous KOH electrolytes of 5 mol dm^{-3}. Each experiment involved a linear potential sweep (LPS) at 2.5 mV s^{-1} from 0.0 V (SCE) to a predefined upper potential.

A conventional three-electrode cell configuration was used employing a platinum counter electrode and a saturated calomel reference electrode (SCE) to which all potentials were referenced. Prior to immersion in the electrolyte, the working electrode was dipped in an etchant (3:1:1 H_2SO_4:H_2O_2:H_2O) for 4 minutes and then rinsed in deionized water. All of the electrochemical experiments were carried out in the absence of light at room temperature.

A CH Instruments Model 650A Electrochemical Workstation was employed for cell parameter control and for data acquisition. Cleaved {011} cross-sections were examined using a HITACHI S-4800 field emission SEM operating at 5 kV. Electron transparent sections for cross-sectional TEM were prepared using a standard focused ion beam (FIB) milling procedures (20) in a FEI 200 FIB workstation. The TEM characterization was performed using a JEOL JEM 2010 TEM operating at 200 kV.

Results and Discussion

Cross-Sectional Electron Microscopy

Figure 1 shows a typical SEM image of a porous layer (011) cross-section after an LPS to a potential where domains of pores have merged into a continuous porous layer beneath a thin dense near-surface layer. Two primary pores that have grown the full extent of the observable porous layer from a pit in the electrode surface are clearly visible. It is clear from the superimposed lines (Fig. 1) representing <111> directions, that these two primary pores have propagated preferentially along the <111>A directions. Measurements of pore width show that these pores have the same width along their entire length except where they appear to narrow near the surface pit and their respective pore tips. Other (shorter) pores are also visible. Pores are observed to grow generally along the <111>A directions, but in some cases deviate from these directions in places. This variation in pore growth direction is most typically observed either where pores are in such close proximity to each other that they have diverged (*e.g.*, at A and D) or when growing towards each other, where they have avoided crossing and actual contact (*e.g.*, at B and C). This tendency of pores to grow around obstacles is frequently observed in images and will be discussed later in the context of the proposed pore propagation model. Even in situations where pores appear to impede each other, such pores appear to have a width that is no greater than the characteristic width of the pores being examined. Furthermore, there is no evidence that the pores are wider when closer to the surface. This consistency in width suggests that pore growth occurs in a specific region, *i.e.* in the vicinity of the pore tips with no subsequent widening due to etching at pore walls in the electrolyte-filled pores.
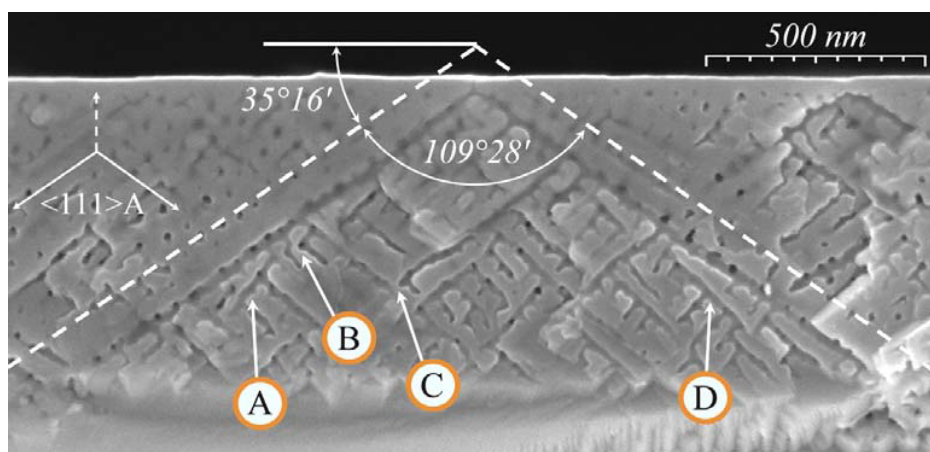
Fig. 1 Cross-sectional (011) SEM image of InP following anodization by LPS to the first current peak in the linear sweep voltammogram (LSV), *i.e.* from 0 to 0.46 V (SCE) at 2.5 mV s^{-1} in 5 mol dm^{-3} KOH. The <111> directions are superimposed on the image as white, dotted lines. Two primary pores extending from a pit in the surface are clearly seen to have propagated along the <111>A directions. Pores that deviate from these directions are indicated at A and D and pores that have avoided crossing each other are indicated at B and C.
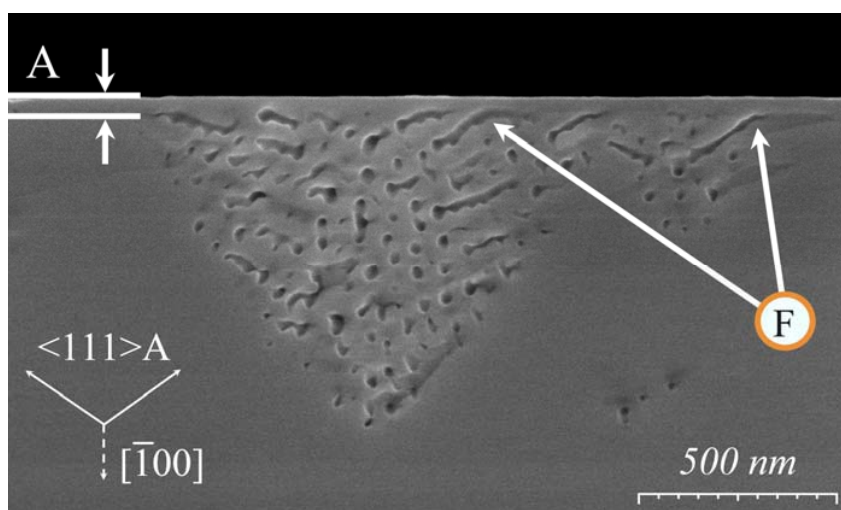

Fig. 2 Cross-sectional SEM image of InP cleaved along the (01$\bar{1}$) plane (orthogonal to Fig. 1) following an LPS from 0 to 0.44 V (SCE) in 5 mol dm^{-3} KOH at 2.5 mV s^{-1}. The pores shown in Fig. 1 (Type 1) appear as round cross-sections. The near-surface layer at A is also visible. Pores in the plane of the image (Type 2) propagate upwards at ~35° to the horizontal plane along the <111>A directions. Two pores that have deviated from the <111>A directions as they approached the near-surface layer are indicated at F.

Figure 2 shows an SEM image of the cleavage plane orthogonal to that shown in Fig. 1. During anodization, the potential sweep was stopped at an earlier potential (*i.e.* at 0.44 V), before the domains had time to fully merge. Therefore, the characteristic triangular (01$\bar{1}$) cross-sections associated with these domains (15) are visible. Two types

of pores are evident: those passing through the $(01\bar{1})$ plane of the image (Type 1) and those in the $(01\bar{1})$ plane of the image (Type 2). The Type 1 pores, which appear as round cross-sections in Fig. 2, have grown within (011) planes (such as that in Fig. 1) orthogonal to the $(01\bar{1})$ plane of the image. Each of the Type 2 pores can be seen to have originated at a Type 1 pore and to have grown along a <111>A direction towards the surface (*i.e.* upward growth at ~35° to the horizontal plane in Fig. 2). Where pores come close to the near-surface layer (*e.g.* at F) they deviate from the <111>A directions leaving the near-surface layer intact. Indeed, most Type 2 pores in Fig. 2 deviate from the <111>A directions due to the proximity of Type 1 pores.
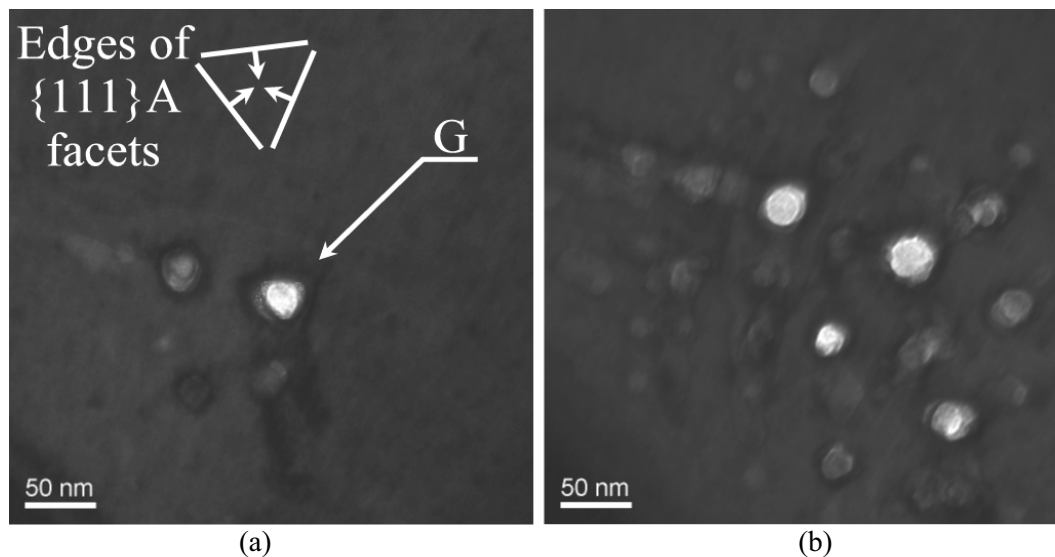

(a)   (b)

Fig. 3 TEM images, viewed along a <111>B direction, of a $(01\bar{1})$ slice of InP. The cross-section in (a) passes through a pore close to its tip (at G) while the cross-section in (b) passes through pores far from their tips. The electrode was anodised by an LPS from 0 to 0.44 V (SCE) in 5 mol dm^{-3} KOH at 2.5 mV s^{-1}. The FIB-milled InP slice is ~100 nm thick.

Pore Cross-Section and Tip Shape

Figure 3 shows two TEM images acquired after tilting the sample so as to observe the pore cross-sections as viewed along a zone axis equivalent to the <111>B direction. The cross-section in Fig. 3a passes close to the apex of a porous domain and intersects a pore very close to its tip (at G). The light-grey triangular area at G appears to be partly faceted. If the facets are considered to form a triangle, the sides are approximately parallel to the intersections of the {111} planes with the image plane as shown in the inset. Thus, the internal surface of the tip of a pore appears to consist of {111}A facets (the arrows in the inset represent the components of the <111>A directions in the image plane). The cross-section shown in Fig. 3b intersects pores at extended distances from their tips. It is clear that, in contrast with Fig. 3a, these cross-sections are quasi-circular and do not show any indication of faceting.

Figure 4 shows an SEM image of a (011) cross-section through a porous domain. Several interesting features of the pores can be observed in this image. As in Fig. 1, a primary pore can be seen at V. The pore has propagated along a <111>A direction and has rough but parallel edges. The parallel edges of this pore can be seen to end at a tip

with a rounded point at T. This is in agreement with TEM images that show partial faceting in pore cross-sections taken near a pore tip (*i.e.* Fig. 3a). Again, it can be seen that not all pores propagate exclusively along a <111>A direction. This is especially the case where pores are branching from a primary pore and are in close proximity to regions that are depleted of carriers by the presence of nearby pores. An example can be observed at S, where a pore has diverged from the primary pore at V. Also, at I, in Fig. 4, a pore that is restricted by several neighbouring pores (such as those indicated by J) has propagated into a bottle-neck resulting in a tapered shape. Again, at K, restriction of the development of a branching pore from V has resulted in pore width narrowing, presumably due to the proximity of other pores not visible in the cross-section but existing in a parallel (011) plane. Despite this narrowing, the pore later re-established itself to a normal width after growing past the impeded region.
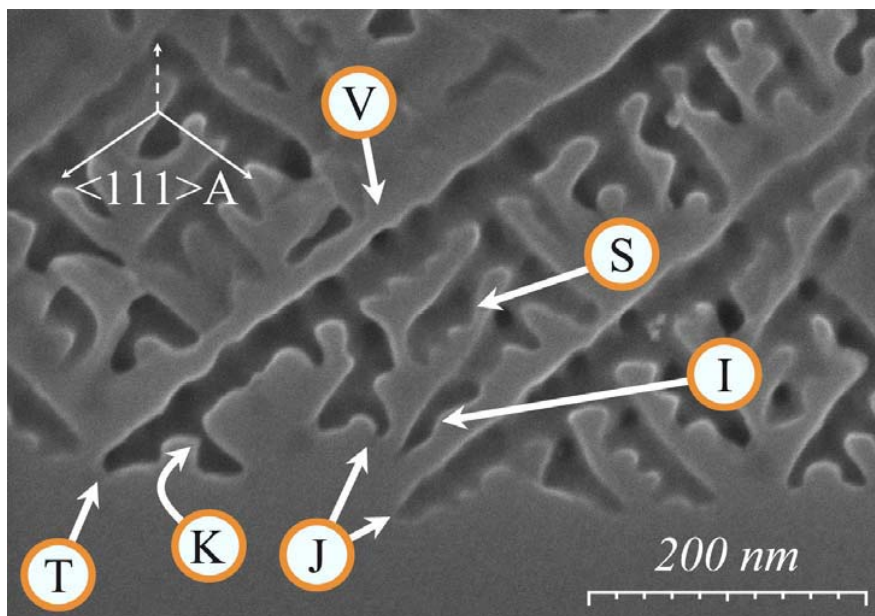

Fig. 4 Cross-sectional (011) SEM image of InP after an LPS from 0 to 0.383 V (SCE) in 5 mol dm^{-3} KOH at 2.5 mV s^{-1}. A primary pore with a tip at T is indicated at V. Pores whose growth has been restricted are indicated at K and I while a pore that has diverged from V is indicated at S.

The observation of a uniform pore width in Fig. 1 is also consistent with the fact that no particular crystallographic facets have been observed along the pore walls; as far as can be determined, the pore cross-sections are round with no apparent facets, except in the vicinity of the tip. If etching occurred at the pore walls as well as at the pore tip, it might be expected that the walls would be faceted, giving a characteristic pore shape such as a triangular cross-section (as is typically observed for etched zinc-blende crystals). For example, Osaka *et al.* (21) reported that pores formed along the <100> directions during etching of silicon in HF solution had square cross-sections, delineated by the {100} planes, and Spiecker *et al.* (22) also reported faceting of pore walls for InP in acidic solution, where the pore cross-sections were triangular and the pore propagation was along <111> directions. However, in both cases, pore width tapered (decreased) with distance towards the pore tip. In the present case of anodic etching of InP in KOH, the preferential etching process occurs only in a very small volume near the pore tip and

this region of reaction is constantly advancing in space. Therefore, the etching process does not delineate pore wall facets. Furthermore, since etching only occurs near the pore tips, the KOH system allows purely electrochemical pore formation to be studied in detail.

Thus, pores propagate preferentially along the <111>A crystallographic directions and have a characteristic pore width but may change direction (and width) so as to navigate past restricted regions of material. As will be shown next, such behaviour can be understood if it is assumed that the etching at the pore tip is controlled both by the high electric field (35), and by preferential etching of the {111}B phosphorus planes.

Preferential Etching and the Three-Step Charge Transfer Mechanism

In III-V semiconductors, the {111}B planes (*e.g.* the phosphorus planes in InP) are commonly found to be fast-etching both in electrochemical pore formation (22,23) and in wet etching of trenches (24). Therefore the direction of etching (*i.e.* the direction in which an etch front moves) is the <111>A direction. Gatos and Levine (25,26) proposed a model for chemical etching of III-V semiconductors with a zinc-blende structure. According to this model the etch rates of these surfaces are dependent on the relative reactivity of the terminating atoms. The {111}A plane is terminated by weakly reacting Group III (metallic) atoms and the {111}B plane is terminated by strongly reacting Group V (non-metallic) atoms. Subsequent work by Holt (27) on the behaviour of these surfaces in InSb supports this model, showing a strong reactivity for the Sb and a weaker reactivity for the In. Research on the behaviour of GaAs (28,29) and InP (30,31) in a range of etchants, such as Piranha (H_2SO_4-H_2O_2-H_2O mixtures) and bromine-methanol, has identified the {111}A planes as the slow etch planes (*i.e.* the planes that are revealed during chemical etching). Similar results for photo-electrochemical etching (32,33) and thermal decomposition (34) of InP also show that the {111}A planes are revealed due to the preferential removal of phosphorus atoms.

It is generally accepted that pore propagation in highly doped n-type semiconductors ($> 10^{18}$ cm^{-3}) is controlled both by the availability of charge carriers at the pore tips and by the strength of the electric field that enables transport of these carriers across the depletion layer that surrounds the tips. The faster etch rate of InP {111}B faces is considered to be due to the full dangling bonds that extend from the phosphorus terminated surface (25,36). Near the pore tips the electric field is sufficiently high to enable substantial tunnelling of carriers (37) and dangling bonds can facilitate a higher etch rate (38).

Modelling of the relationship between pore-tip shape and electric field in silicon by Zhang (35) showed that the electric field is dependent on the radius of curvature of the internal surface of a pore. He concluded that the electric field ξ at the surface is a function of the ratio of the radius of curvature r_o and the space-charge layer thickness x_{sc}, *i.e.* $\xi = \xi(r_o/x_{sc})$. Since a threshold electric-field ξ_{min} must be attained for hole supply to occur, a corresponding threshold value Λ of r_o/x_{sc} must also exist. Thus, a reduction in x_{sc} corresponds to a reduction in the value of r_o at which the threshold values of Λ and ξ_{min} are attained. One must be careful in routinely assigning this mechanism to any and all pores in etched III-V semiconductors, but the limited and controlled supply of holes in this case is most likely a true explanation of the mechanism of preferential pore growth; no pores are observed in p-type InP electrodes or low doped (~5 × 10^{17} cm^{-3}) InP anodized in similar KOH solutions (18), and furthermore, a uniform supply of holes at a surface would not result in pore growth or pitting, but electropolishing.
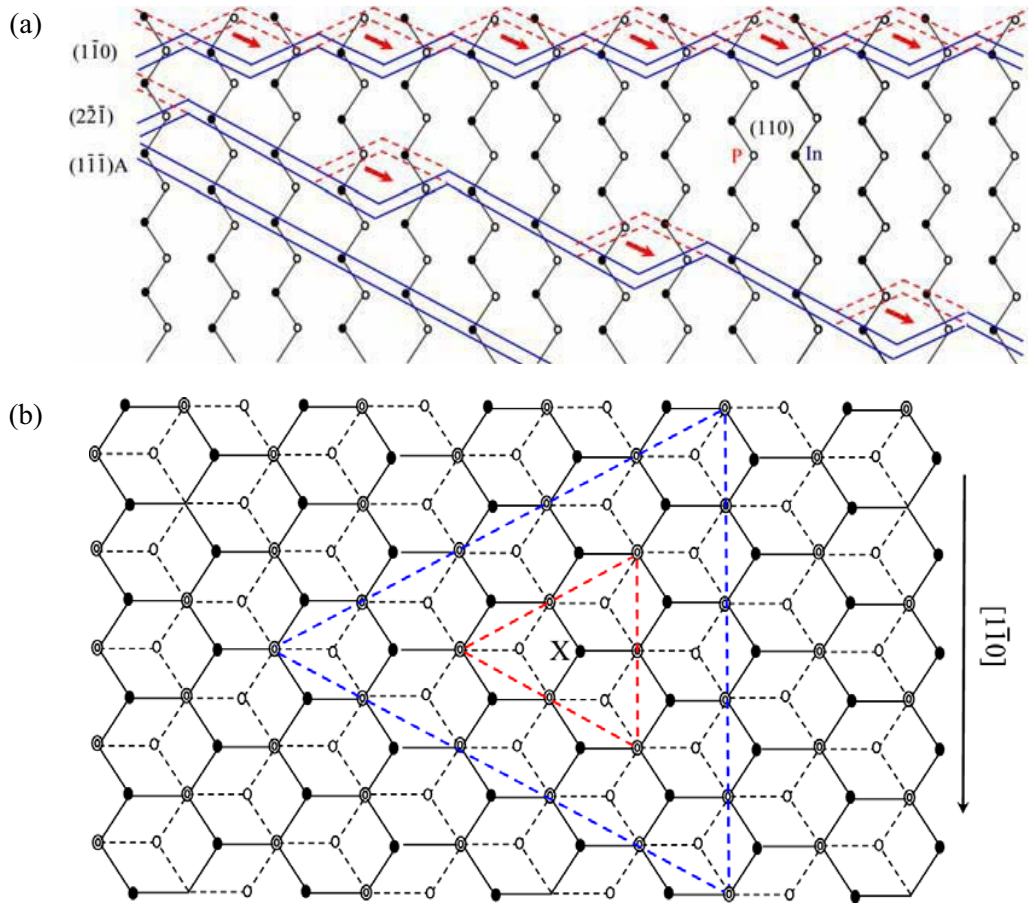
Fig. 5 (a) A (110) section of a zinc blende lattice showing minimum dangling bond construction of three planes with a [110] zone axis: $(1\bar{1}0)$, $(2\bar{2}\bar{1})$ and $(1\bar{1}\bar{1})$A. Arrows indicate the direction of etching. (b) Plan view of (111)A surface of a zinc blende lattice. Solid lines represent bonds between surface atoms. Fine dashed lines represent bonds between atoms in the second layer. Double circles indicate inter-planar bonds (from a white atom) to an underlying (black) atom. Bold dashed coloured lines indicate the progression of etching after the removal of atom X. Black atoms = Indium. White atoms = Phosphorous. (Diagrams are from work by D. N. MacFayden (38).)

A mechanism of chemical etching has been described by MacFayden (38) where it was proposed that chemical etching progresses through the removal of the most loosely bound atoms from the crystal faces. In the case of III-V semiconductors, the {111}B terminating atoms (e.g. phosphorus) are the most loosely bound. Atomic ledges that exist on any surface represent quasi {111}B planes, as shown in Fig. 5a. Since these are the fast-etching planes, it is proposed that the ledges etch, revealing a fresh {111}A plane one monolayer beneath the original. Such a method is depicted schematically in Fig. 5a. Where such a {111}A plane has been revealed, there are no {111}B atoms remaining, but where a single In atom is removed from such a plane, a triangular-shaped void, one atom deep, surrounded by a ledge of {111}B phosphorus atoms, is revealed, as shown at X in Fig. 5b. The phosphorus atoms on this ledge can then be etched, revealing loosely bound indium atoms (*i.e.* atoms bonded to the crystal by only two bonds) which in turn can be

easily etched to reveal a similar, but widened, triangular-shaped void in the {111}A surface surrounded by a ledge of {111}B phosphorus atoms (as in Fig. 5b). Therefore an indium vacancy in a {111}A surface allows a layer of atoms to etch quickly, in a 'zip-like' fashion, as shown in Fig. 5b. This relatively rapid etching occurs instantaneously in two dimensions, outwards from the initial indium vacancy (at X), exposing the next {111}A plane; the crystal can be considered to comprise of a stack of 2-D {111}A layers (planes) that are removed one at a time revealing the next {111}A layer to be etched.
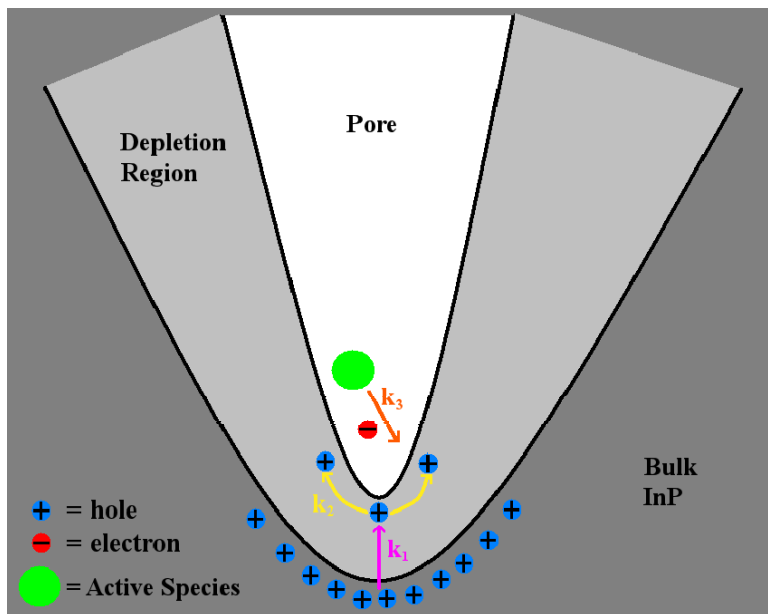

Fig. 6 Schematic representation of the three-step charge transfer model at a pore tip. K_1 represents the rate at which holes are supplied to the pore tip. K_2 represents the characteristic diffusion time for holes at the electrode/electrolyte interface. K_3 represents the rate at which the active species in the electrochemical reaction captures holes from (injects electrons into) the interface.

Crystallographic oriented pore growth can be considered a combination of the two etch mechanisms presented above *i.e.* preferential hole supply at the pore tips and preferential etching of {111}B surface sites. An understanding of why pores would propagate along the <111>A directions can be obtained by consideration of a general model for charge transfer across the semiconductor/electrolyte interface. This model argues that the charge transfer process involves three key steps (as shown in Fig. 6). The first step is rate limiting, and is the supply of holes to the semiconductor surface. This, as has already been argued, can occur only at the pore tip. Once holes arrive at the pore tip, they have some time to diffuse at the electrode surface, via the valence band and surface states, before taking part in the electrochemical reaction with the active species in solution. The hole diffusion and the hole annihilation in the electrochemical reaction are the second and third steps in the charge transfer, respectively. While the rate at which CO pore etching occurs would not be affected by these two steps, both the spatial extent of the reaction (pore width), and the degree of preferential etching would be affected.

For example, if the rate of the third step with respect to the second step were to increase – *e.g.* due to increase in the activity of the electrolyte – then the pores would

become narrower. However, if the solution was to become less active, the pores would widen. Indeed, this widening of the pore tip, by the mechanism of the second step (hole diffusion at the pore tip), to a width greater than that due to the region of enhanced electric field, is essential for crystallographic growth to occur. This is because in the region where the electric field is high there is a large supply of free carriers (holes). Therefore in this region of the electrode-electrolyte interface, the electrolyte can etch any site. However, away from this region holes must diffuse from the region of high tip-curvature, resulting in a lower hole density with distance from the tip. Therefore, away from the tip, sites where holes become trapped become more likely to etch than the surrounding sites.

It follows that diffusion of holes at the semiconductor surface is necessary for the preferential etching of {111}B planes, as in the mechanism of MacFayden. If the holes were annihilated instantly upon arrival at the surface, pores would be expected to propagate along random directions, loosely aligned to the source of holes. The {111}B surface states would not necessarily provide a preferential site into which a hole would tunnel, since tunnelling probability is most strongly related to the width of the barrier (35). However, the {111}B surface states could act as long-lived 'trap' states. Therefore, under suitable conditions, electron injection from the solution should be more likely to take place at these sites leading to preferential etching and the revealing of {111}A slow-etch planes near (but not at) the pore tips.

The minimum pore width is determined primarily by the width of the region of enhanced electric field that is present at the pore tip. Since the region surrounding the pore tip is depleted of carriers, any carrier that arrives at the pore tip must have tunnelled there from the bulk semiconductor. This is only likely near the pore tip where the electric field is enhanced. If, once holes arrive at the pore tip they instantly take part in the electrochemical reaction, the measured pore width would be determined exclusively by the ratio r_o/x_{sc} as described earlier. However, if the holes have some time to diffuse away from this region, then the spatial extent of the electrochemical reaction would be increased, and wider pores would be observed. The pore width of an isolated pore is therefore determined by three factors; (i) the ratio r_o/x_{sc}, (ii) the diffusion rate of holes at the semiconductor surface and (iii) the kinetics of the electrochemical reaction (which determine how long a hole will exist on the surface before being annihilated). Analysis of these factors is examined in greater detail by Quill *et al.* (8,11,17)

Pore Propagation Mechanism

Now that the three-step charge transfer mechanism has been described, and the justification for the revealing of the {111}A planes (*i.e.* selective etching of {111}B atoms) has been presented, branching and the growth of <111>A oriented pores will be considered in more detail.

Consider an electrolyte-filled void in a semiconductor. At the semiconductor-electrolyte interface, under suitable conditions of electric field, carrier concentration and electrolyte composition, the 'zip-like' propagation of etching described by MacFayden will eventually reveal {111}A facets. These facets will enlarge in area until they meet, creating a tetrahedral shape as shown in Fig. 7a. As etching continues, the tetrahedron will increase in volume. Due to the relationship between depletion layer width and surface curvature, the electric field across the interface will vary with position on the surface of the tetrahedron, being greatest at the apexes and decreasing towards the centres

of the faces. Etching would not necessarily be restricted solely to regions in which the electric field is above ξ_{min}. The diffusion of holes at the surface would result in an increase in the spatial extent of etching beyond that dictated by ξ_{min}. In this way, the minimum size of a tip where hole supply can occur is dictated by ξ_{min}, but the actual size of the tetrahedral void that extends from the four tips also depends on both the rate of hole diffusion at the surface and the kinetics of the electrochemical reaction (steps two and three of the charge transfer model in Fig. 6, respectively). It follows that, as the tetrahedron grows, holes will no longer be able to reach the centres of the four {111}A facets; both the electric field and the hole diffusion will be insufficient to maintain etching. Therefore, etching will cease in those regions while the remainder of the void (closer to the vertices) will continue to etch. This situation is shown in Fig. 7b, where continued etching of void walls has resulted in the formation of the tips of four new pores that are directed outwards from the vertices.
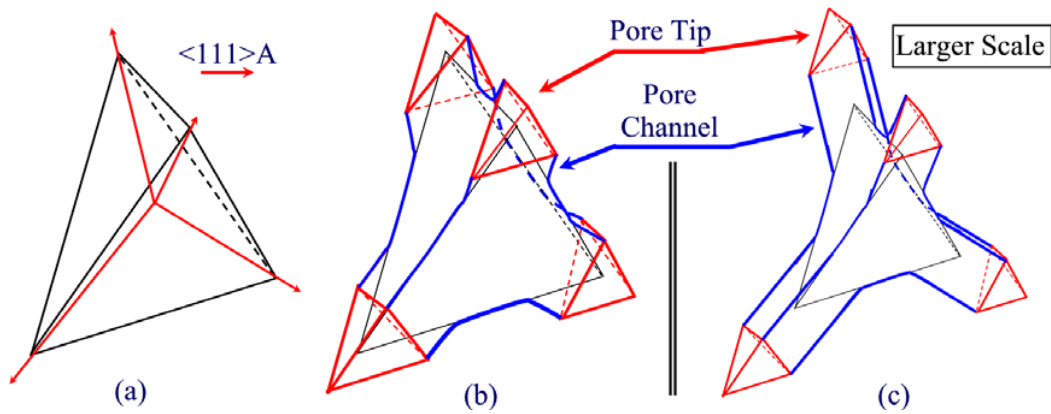

Fig. 7 Schematic representation of the widening of a hypothetical electrolyte-filled void in the bulk of the zinc-blende InP crystal. (a) The etching initially results in a tetrahedral void. (b) As the void becomes larger, suitable conditions for etching continue to exist only at the vertices. Therefore (c) the void stops expanding while four pore tips grow outwards from the vertices along the <111>A directions.

'Zip-like' etching will occur on the {111}A facets near the tips of these pores, maintaining the vertex of each tip. The tip itself should not be faceted since the large supply of holes at the tip should result in all sites etching at a similar rate. However, a short distance away from a tip the decrease in the density of free carriers (holes) should result in preferential etching of sites where the holes are trapped. If the supply of holes at the three {111}A facets is equal, etching will progress at the same rate at each facet (since they are equivalent) resulting in the propagation of each pore tip along a <111>A direction (*i.e.* in the direction of the sum of the vectors). In the absence of these three stabilizing vectors (that result from the 'zip-like' etching of the three facets) the tip would wander. However, not alone do the facets stabilize the propagation direction they also sharpen the tip and therefore if a tip wanders away from <111>A propagation it will be dragged back both by the zip-like etching and by the resulting etch vectors of the three facets.

In the wake of each tip (in the direction away from the tip), etching will also occur until the electric field becomes too small and diffusion of carriers at the interface becomes insufficient. Therefore the channels of the pores are limited to a characteristic width. The locus of the threshold electric field and therefore of the diffusion of carriers

on the {111}A facets is such that the resulting pore cross-section is approximately circular. The walls of a channel in the wake of the propagation of each tip will not etch further since the electric field strength is too low to maintain tunnelling-mediated etching (see Fig. 7c).
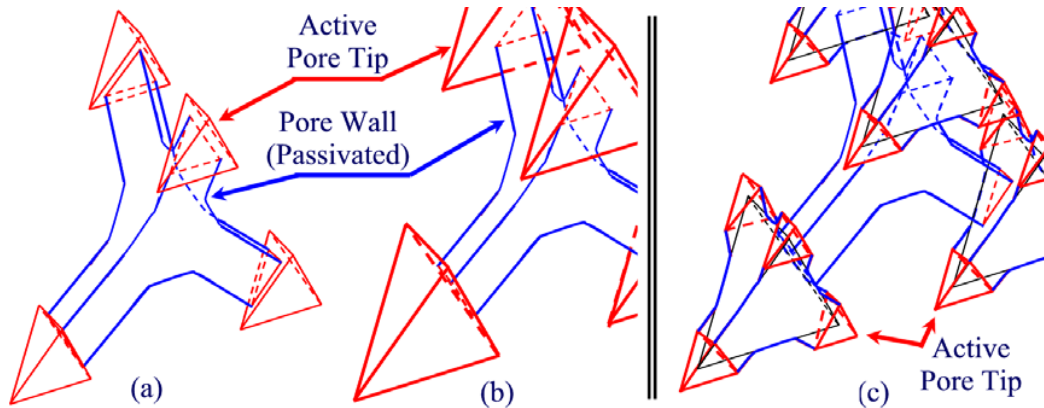

Fig. 8 Schematic representation of the widening of pore tips (a) after the tip has extended past the depletion region of the void from which it originated. This is followed by (b) the expansion of these tips into tetrahedral voids until, as in Fig. 7, suitable conditions for etching continue to exist only near the vertices and where the pore tips form. This expansion of the pore tips leads (c) to branching of the pores along the <111>A directions.

To the rear of the growing tip structure, the availability of carriers is limited due to the proximity of the depletion region surrounding the void. Once the pore tip has progressed some distance from the starting point, carriers become available that (along with the slight variations in pore propagation direction) allow the formation of a fourth <111>A facet to the rear of the propagating tip. The tip structure itself now has up to three additional vertices (*i.e.* a total of four corresponding to the four <111>A directions as shown in Fig. 8a). Thus, the tip structure now has a tetrahedral shape which expands until the combination of enhanced hole supply at the vertices and hole diffusion from the vertices becomes unable to supply holes to the centres of the tetrahedron's sides (Fig. 8b). As etching continues near the vertices, pore tips appear at each of the four vertices, as depicted in Fig. 8c. Thus, a porous structure is formed by pores that propagate and branch solely along the <111>A directions.

As depicted in Fig. 7c, a pore can propagate along the <111>A direction because the {111}A facets near the tip are etched at equal rates and the three facets sharpen and point the tip in the <111>A direction. This is possible when carrier availability is present to equal degrees at all three {111}A facets. If it is diminished at any of the three tip facets, the etch rate at that facet decreases, causing the propagation of the pore tip to deviate (or be dragged) away from that facet. Thus, when the tip of a pore is close to existing pores – and the pores are separated by a distance less than the sum of the widths of their depletion layers – an absence of carriers is caused by the overlapping of the depletion layers, resulting in the redirecting of the pore away from adjacent pores and from its original <111>A growth direction. The outcome of such a process can be seen at S in Fig. 4 – where the pore tip has veered away from the pre-existing pore channel at V – and at F in Fig. 2 – where pores have veered away from the bulk electrolyte creating a near-surface layer of thickness A.
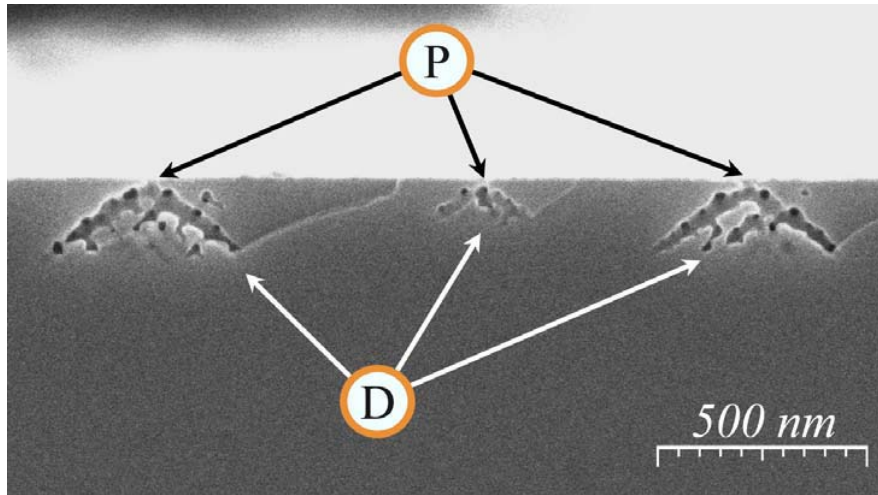
Fig. 9 Cross-sectional (011) SEM image showing pits at P that connect the surface to two primary pores. The n-InP electrode was anodized in 5 mol dm^{-3} KOH by a LPS from 0 to 0.245 V (SCE) at 2.5 mV s^{-1}.

A similar situation arises at the surface pits. The cross-section of an InP electrode after the early stages of pore development in Fig. 9, shows two sets of pores and the surface pits from which they originate. Such pits (which form channels through the near-surface layer) are oriented along the [$\bar{1}$00] direction, and connect the surface (*i.e.* electrolyte) to the underlying porous domains. This is depicted schematically in Fig. 10. Once a surface pit has formed, its preferred shape is, like that of any void in this system, a tetrahedron. However, the majority of carriers (holes) are generated by a tunnelling mechanism through the associated depletion layer at the surface, and this can occur only at small angles to the surface normal, corresponding to regions in space where the depletion layer is thin enough to promote carrier tunnelling through a (locally) higher electric field, as shown at x and y in Fig. 10a. Thus, etching at the surface pit is initially primarily constrained to be normal to the surface causing the formation of a very narrow channel, as shown in Fig. 10b. Once a channel (formed from a surface pit) has grown a certain distance through the depletion layer, the availability of carriers at the sides of the channel tip allow the formation of {111}A oriented facets and the formation of a truncated tetrahedron shape at the tip of the channel, as shown in Fig. 10c and can be seen for actual domains at D in Fig 9. This truncated tetrahedron continues to expand (Fig. 10e) until the electric field near the centres of its facets becomes insufficient to sustain etching, while etching continues near the vertices. This results in the formation of two primary pores as shown in Fig. 10e. As shown at P in Fig. 9 the mechanism etches narrow channels along the [$\bar{1}$00] direction through the near-surface layer that widen to form two primary pores from each pit. Similarly, the channel formed during the restricted growth of the pore at K in Fig. 4 can be explained by the propagation of a pore tip through a similarly wide depletion region that exists between two pre-existing pores, which themselves are not parallel to the propagation direction of the new (branching) pore tip.
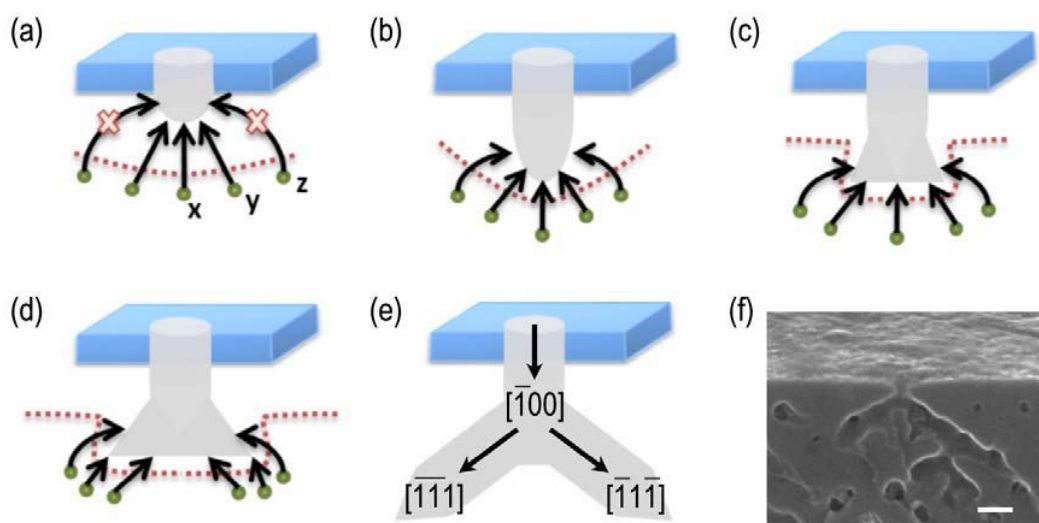
Fig. 10 Schematic representation of the progression of etching from a pit in the surface. Firstly, (a) the lower surfaces of this pit preferentially etch vertically downwards due to increasing availability of carriers with decreasing angle to the surface normal (from y to x). This etching results in the formation (b) of a long, narrow channel in the [$\bar{1}$00] direction. Once the channel is deep enough, the availability of carriers to the sides allows some lateral etching (c). This etching widens the end of the channel into a truncated tetrahedral void that produces (d) two primary pores when the void is sufficiently large (e). The model can be directly compared to experimental observation of pore growth initiation (scale bar = 50 nm) (f).

Carrier Concentration Influence on Porous Domain Dimensions

The carrier concentration of the n-InP has a major effect on the electrochemical process resulting in changes in the magnitude and position of current peaks and in the overall shape of linear sweep voltammograms (LSVs) (16).

Table I. Variation, due to carrier concentration of InP, of average values for three porous layer parameters: surface pit diameter, near-surface layer thickness and pore width.

Carrier Concentration / $\times 10^{18}$ cm^{-3}	Surface Pit Diameter / nm	Near-Surface Layer Thickness / nm	Pore Width / nm
3.4	14	45	30
5.3	17	39	28
6.7	22	34	19

Table I shows how several porous layer parameters vary with carrier concentration, experimentally determined for three highly doped n-InP electrodes. With increasing carrier concentration, surface pit diameter increases and both the near-surface-layer thickness and the pore width decrease. Although the variation of these parameters is not large, this is a very interesting result since it suggests a relationship between the mechanisms that determine respectively the thickness of the near-surface layer and the pore width, while also suggesting that the surface-pit diameter and the pore width are not directly related.

To explain the variation of the parameters in Table I, it is useful to consider the width x_{sc} of the depletion layer at the semiconductor solution interface. For a given potential difference across the interface, the depletion layer must decrease with increasing carrier concentration. This variation in x_{sc} can help explain the data in Table I since the pore growth mechanism is dependent on the tunnelling of carriers across the depletion layer. However, the explanation for the observed increase in pit diameter with increasing carrier concentration is not entirely obvious.

The pore wall and near-surface layer thicknesses are influenced by the redirection of pore growth away from regions of limited carrier availability. As discussed earlier, this process occurs where the depletion layers of two neighbouring pores overlap. The pores will, of course, etch with a greater rate in directions where carriers are available, with the result that tips propagate away from, or around, existing pores (and the bulk electrolyte). Therefore, at higher carrier concentrations, the depletion layer is thinner and consequently pores can grow much closer together, decreasing the thickness of both the inter-pore walls and the near-surface layer.

As explained earlier, a threshold electric field ξ_{min} must be attained for etching to take place, and a corresponding limiting value Λ of r_o/x_{sc} also exists. Therefore a decrease in x_{sc} must be matched by a proportionate decrease in r_o so as to maintain the value of Λ. Since the value of x_{sc} at a given potential decreases with increasing carrier concentration, the radius of curvature of the pore tip must also decrease resulting in a decrease in pore width.

The pit diameter does not increase as x_{sc} increases, instead it decreases. Geometrical considerations suggest that this trend may simply be due to an effect that causes the surface pits to widen as the thickness of the near-surface layer decreases. That is, for a narrower near-surface layer (and narrower depletion-layer width, x_{sc}), a greater variation in the angle of propagation-of-etching-away-from-the-normal-to-the-surface is allowed. This reduction in the restrictions on etching direction allows the channel from the pit to widen while still remaining smaller than the characteristic diameter of the pores that grow in the domain that it connects with the bulk electrolyte.

Conclusions

Observation of pores and their cross-sections, using SEM and TEM, shows that pore tips are partly faceted with {111}A internal faces and propagate along the <111>A directions, deviating from this direction due to the proximity of neighbouring pores. Such deviations occur where the availability of carriers is reduced when the depletion region surrounding a tip overlaps another region that is depleted of carriers. Despite the tip shape being faceted, the pore cross-sections are round and the pore width is constant with respect to distance from the tip, *i.e.* the pore channels are quasi cylindrical in shape.

We have presented a mechanism for pore formation which proposes that charge transfer between the semiconductor and the electrolyte involves three key steps. The first step is the supply of holes to the pore tip and this is typically the rate limiting step. Once holes arrive at the surface they have some time to diffuse (step two) before being annihilated in the electrochemical reaction (step three). The holes diffusing at the surface would tend to become 'trapped' at {111}B surface states in the band gap, leading to preferential etching at these sites. The {111}A faces near the tip are then revealed due to fast etching of loosely bound {111}B phosphorus atoms resulting in an etch process where removal of planes of atoms parallel to the {111}A facets begins with an indium

vacancy in a {111}A face. The vertex of a pore tip is therefore maintained where the three {111}A facets intersect; this in turn maintains a sufficient electric field strength near the tip due to the high surface curvature in this region. To the rear of the tip, the electric field decreases below the threshold value required for etching and the locus of the threshold electric field and carrier diffusion length on the {111}A facets is such that the resulting pore cross-section is approximately circular. Where the availability of carriers is reduced near one of the facets at a pore tip, etching is reduced at the facet causing pore growth to deviate from the <111>A direction and away from the facet where further growth has been limited. This also results in changes in the shape of a tip and the channel that is left in its wake.

Compared to porous semiconductor formation in acidic solutions, pore growth in the high *p*H electrolyte of KOH is controlled by the availability of carriers through a mechanism involving solely electric-field-generated carrier-tunnelling (which is tuned by the InP dopant density and type) at the pore tips. It follows that no observable chemical etching takes place at the pore walls. In fact, all electrochemical etching occurs at the pore tips.

The quantitative experimental data coupled with a qualitative mechanism provide a solid description of the pore growth process in InP anodized in KOH. The mechanism comprehensively explains why pore growth occurs preferentially along the <111>A crystallographic directions while describing how deviation from these preferential growth directions can occur when pores are in close proximity to other pores or depleted regions of the semiconductor. Furthermore, the model describes, and is in agreement with, the variation of porous layer parameters with extrinsic carrier concentration of the InP.

References

1. R. L. Smith and S. D. Collins, *J. Appl. Phys.*, **71**, 8 (1992)
2. S. Langa, J. Carstensen, M. Christophersen, H. Föll, and I. M. Tiginyanu, *Appl. Phys. Lett.*, **78**, 1074 (2001)
3. G. Oskam, A. Natarajan, P. C. Searson, and F. M. Ross, *Appl. Surf. Sci.*, **119,** 160 (1997)
4. S. Langa, J. Carstensen, I. M. Tiginyanu, M. Christophersen, and H. Föll, *Electrochem. Solid-State Lett.*, **4**, G50 (2001)
5. S. Langa, I. M. Tiginyanu, J. Carstensen, M. Christophersen, and H. Föll, *Electrochem. Solid-State Lett.,* **3**, 514 (2000)
6. P. Schmuki, J. Fraser, C. M. Vitus, M. J. Graham, H. S. Isaacs, *J. Electrochem. Soc.,* **143,** 3316 (1996)
7. P. Schmuki, D. J. Lockwood, J. Fraser, M. J. Graham, H. S. Isaacs, *Mater. Res. Soc. Symp. Proc.,* **431,** 439 (1996)
8. N. Quill, R. P. Lynch, C. O'Dwyer and D. N. Buckley, *ECS Trans.*, *this volume* (2012)
9. A.-M. Gonçalves, L. Santinacci, A. Eb, I. Gerard, C. Mathieu and A. Etcheberry, *Electrochem. Solid-State Lett.*, **10** (4), D35 (2007)

10. R. P. Lynch, C. O'Dwyer, D. N. Buckley, D. Sutton and S. B. Newcomb, *ECS Trans.*, **2,** 131-141 (2006)

11. N. Quill, R. P. Lynch, C. O'Dwyer and D. N. Buckley, *Proceedings of Pits and Pores 5: A Symposium in Honor of David Lockwood, Honolulu PRiME 2012*, Abstract 2420

12. M. Christopherson, J. Cartensen, A. Feuerhake, and H. Föll, *Mater. Sci. Eng. B,* **69,** 70, 194 (2000)

13. S. Rönnebeck, J. Carstensen, S. Ottow, and H. Föll, *Electrochem. Solid-State Lett.,* **2**, 126 (1999)

14. P. Schmuki, L. E. Erickson, D. J. Lockwood, J. W. Fraser, G. Champion, H. J. Labbé, *Appl. Phys. Lett*., **72**, 1039 (1998)

15. R.P. Lynch, C. O'Dwyer, D. Sutton, S. B. Newcomb, and D. N. Buckley, *ECS Trans.*, **6** (2), 355 (2007)

16. C. O'Dwyer, D. N. Buckley, D. Sutton, M. Serantoni, and S. B. Newcomb, *J. Electrochem. Soc.*, **154**, H78 (2007)

17. N. Quill, R. P. Lynch, C. O'Dwyer and D. N. Buckley, *Proceedings of Pits and Pores 5: A Symposium in Honor of David Lockwood, Honolulu PRiME 2012*, Abstract 2421

18. C. O'Dwyer, D. N. Buckley, D. Sutton, and S. B. Newcomb, *J. Electrochem. Soc.,* **153**, G1039 (2006)

19. R. P. Lynch, M. Dornhege, P. Sánchez-Bodega, H. H. Rotermund, and D. N. Buckley, *ECS Trans.*, **6** (2), 331 (2007)

20. L. A. Giannuzzi and F. A. Stevie, *Micron.*, **30**, 197 (1999)

21. T. Osaka, K. Osgasawara, and S. Nakahara, *J. Electrochem. Soc.,* **144**, 3750 (1991)

22. E. Spiecker, M. Rudel, W. Jäger, M. Leisner and H. Föll, *phys. stat. sol. (a),* **202,** 2950 (2005)

23. S. Langa, J. Carstensen, I. M. Tiginyanu, M. Christophersen, and H. Föll. *Electrochem. Solid-State Lett.,* **5**, C14 (2002)

24. M. Kappelt and D. Bimberg, *J. Electrochem. Soc.*, **143**, 3271 (1996)

25. H. C. Gatos and M. J. Lavine, *J. Electrochem. Soc.,* **107**, 427 (1960)

26. H. C. Gatos, *J. Appl. Phys.,* **32**, 1232 (1961)

27. D. B. Holt, *J. Appl. Phys.,* **31**, 2231 (1960)

28. Y. Tarui, Y. Komiya and Y. Harada, *J. Electrochem. Soc.,* **118**, 118 (1971); S. Iida and K. Ito, *J. Electrochem. Soc.,* **118**, 768 (1971)

29. S. Adachi and K. Oe, *J. Electrochem. Soc.,* **130**, 2427 (1983)

30. P. H. L. Notten, *J. Electrochem. Soc.,* **138**, 243 (1991)

31. I. E. Vermeir, W. P. Fomes, and P. van Daele, *J. Electrochem. Soc.,* **142**, 3226 (1995)

32. D. Soltz and L. Cescato, *J. Electrochem. Soc.,* **143**, 2815 (1996)

33. M. M. Carrabba, N. M. Nguyen, and R. D. Rauh, *J. Electrochem. Soc.,* **134**, 1855 (1987)

34. S. N. G. Chu, C. M. Jodlauk, and W. D. Johnston, Jr., *J. Electrochem. Soc.,* **130**, 2399 (1983)

35. X. G. Zhang, *J. Electrochem. Soc.,* **138**, 3750 (1991)

36. M. Nishida, *J. Phys. C,* **12**, 535 (1981)

37. X. G. Zhang, *J. Electrochem. Soc.,* **151**, C69 (2004)

38. D. N. MacFayden, *J. Electrochem. Soc.,* **130**, 1934 (1983)

39. S.M. Sze, Physics of Semiconductor Devices, 2nd ed., Wiley, New York**,** (1981)